International Journal of Solids and Structures 47 (2010) 1838–1846

Contents lists available at ScienceDirect

International Journal of Solids and Structures

journal homepage: www.elsevier.com/locate/ijsolstr

Environmentally assisted initiation and growth of multiple surface cracks

Ulf Hejman [a,*], Christina Bjerkén [a,b]

[a] Div. Mat. Sci., Malmö University, SE-205 06 Malmö, Sweden
[b] Div. Mat. Engng, Lund University, SE-211 00 Lund, Sweden

ARTICLE INFO

Article history:
Received 12 November 2009
Received in revised form 4 March 2010
Available online 30 March 2010

Keywords:
Stress corrosion
Crack initiation
Multiple cracking
Polycarbonate
Three point bending

ABSTRACT

The initial stages of stress corrosion on an amorphous polymer is investigated. This is done by exposing stressed specimens of polycarbonate to an acetone and water solution. The surface develops two distinct features of degradation that appear on different length scales when subjected to tensile stress. Small pits form on the surface and make it rough. These pits are in the order of micrometers, and are found to be randomly distributed. They occur even without load and seem to slightly increase in number with increasing stress. In the millimeter domain, visible to the bare eye, surface cracks are formed transverse to the direction of loading. The occurrence of cracks is seen to have a positive stress threshold value, exceeding which, a linear increase of number of cracks with stress is found. The manners in which the cracks grow and coalesce on the surface are examined. It is seen that they do not meet crack tip to crack tip. Instead, they avoid each other initially and coalesce crack tip to crack side. The results are discussed in the light of mechanical considerations. A stress analysis for a few configurations of meeting cracks supports the experimental observations. With assumptions of stress corrosion crack growth and coalescence, a simulation of cracks growing from randomly distributed initiation sites is performed. Similar crack patterns as obtained in the experiments are found.

1. Introduction

The phenomenon of stress corrosion, SC, has been studied intensively for the last five decades. When subjected to aggressive species in the surrounding environment, stress corrosion cracking, SCC, may occur in many kind of materials. The mechanisms differ for metals, ceramics and polymers, but all materials experience similar signs of attack and cracking. For a list of material and environment combinations, see e.g. Davis (2001). Stress corrosion of metals and associated crack growth due to oxidation is perhaps the most common SCC process where electrochemical processes cause the degradation. A well accepted model to describe the process is by formation of an oxide film that may or may not be protective to the underlying substrate. Repeated breakage of the film makes the crack advance in metals. Often, hydrogen induced cracking is also considered as SCC. In polymers, stress induced degradation is caused by dissolution of material or weakening by bond breakage in the polymer structure. Usually, SCC is divided into three phases with characteristic crack growth mechanisms and crack growth velocities. The initiation phase, followed by a steady state crack growth stage where the crack growth rate is controlled by chemical kinetics and mass transport in the crack and at the crack tip. Crack growth from these mechanisms may occur at low loads, compared with the material's fracture toughness. Finally, an accelerating crack growth, leading to final fracture occurs due to mechanical overload. Over the last fifty years research efforts have been conducted to increase the understanding of the underlying processes. The initiation phase is, however, not as well investigated. Also, it has proven hard to build a theory describing the transition between the different stages. For a general review of the SCC phenomenon, see e.g. Jones (1992, Chapter 1).

One of the first attempts to describe the evolution of a stressed surface was made by Asaro and Tiller (1972) and perhaps the most famous extension to this work was made by Grinfeld (1991, 1993, 1998). They have theoretically shown that a stressed flat surface is thermodynamically unstable, and surface and bulk diffusion as well as dissolution and deposition of material will inevitably lead to roughening of a stressed surface. The phenomenon is knows an Asaro-, Tiller-, Ginfeld-instabilities, or only ATG instabilities. This process is counteracted by the surface energy that tends to flatten a surface. This leads to a surface roughness with a stress dependent characteristic wavelength spectrum. The phenomenon may appear at interfaces subjected to SCC or etching as Asaro, Tiller and Grinfeld considered. It may also be observed at crystal growth, treated theoretically by e.g. Spencer et al. (1992) and at the interface between a solid and its melt by e.g. Grinfeld (1986).

An extension of the theoretical analysis of the developing surface roughness was developed by Yang and Srolovitz (1993). They found that if the surface was allowed to continue to evolve,

* Corresponding author. Tel.: +46406657732; fax: +46406657706.
E-mail address: ulf.hejman@mah.se (U. Hejman).

0020-7683/$ - see front matter © 2010 Elsevier Ltd. All rights reserved.
doi:10.1016/j.ijsolstr.2010.03.023

the initial perturbations of the surface grow into cusp like pits and concluded that this may be a connection between the initiation of cracks and crack growth. In an analysis, Yu (2005) found that a flat surface will develop a roughness and cracks as long as the stress can destabilize the surface. At first the surface roughens and blunt pits, that eventually may sharpen into cracks, grow. This implies that the process does not have a stress threshold value. However, the time for a development to a crack can be significant, and they defined a stress threshold value over which a notch would immediately form and grow into a crack. Sou and Yu (1997) made calculations on a stressed cycloid shaped surface and found that small grooves would grow into a shape where the surface evolve invariantly if the stress is small and, if the stress is large enough, the grooves will instead form sharp cracks. Spencer and Meiron (1994) continued this approach with a nonlinear evolution law and found that singular grooves, cusps, form as a direct result from the nonlinear part. The more irregular the initial surface is, the more pronounced the nonlinearity contribution would be. The solution they found is unambiguous which makes it possible to reverse the approach and get a measure of the stress on the surface by examining the surface roughness wavelength distribution. An experimental procedure for calculating the stress from the wavelength distribution was developed by Kim et al. (1999) and Yu and Sou (xxxx). Grilhé (1993a), on the other hand, found the solution to be multi valued when applying a different technique calculating the energetic driving force for roughness appearance on a free surfaces under stress. See also Grilhé (1993b) and Colin and Grilhé (2005). Finally, Song et al. (2005), Yang (2006) calculated the surface evolution in a thin elastic layer and found the frequency of the surface roughness to be dependent not only on the stress and material properties, such as the modulus of elasticity or surface energy, but also on geometrical factors such as the thickness of the layer.

Simulations of surface evolution using different numerical methods, based on e.g. the finite element (FE) analysis, have been conducted to evaluate the phenomenon. Prevost et al. (2001) developed a numerical technique to analyse and simulate the dissolution and mass transport processes. This procedure can be used for simulating crack initiation under various conditions, e.g. at grain boundaries. However, crack growth is not at all considered. The situation with a growing SC crack has been considered by Jivkov and Ståhle (2002), Jivkov (2004). In this case, the growing crack is driven by dissolution of material due to breakage of a protective oxide film on the body boundary where strain exceeds a threshold value. According to this model, the width of the crack may not be finite, as is found by others mentioned above, and the crack cannot be sharp unless the growth mechanism is changed. This is also seen with SC cracks found in nature. Another interesting result is that the cracks grow in a self similar manner. Ståhle et al. (2007) have used numerical methods for simulation of crack growth from energetic relations and come to the similar results as Jivkov has.

Shreter et al. (1999, 2001) performed etching experiments on mechanically loaded silicon plates. It was found that on a nanometre scale the surface was roughened due to oxidation induced stacking faults. On a micrometer scale, small cracks appeared transverse to the direction of loading. Only compressive load gave signs of attack. The number and length of the visible cracks were found to be increasing with increasing load and no threshold value was found in the experimental results.

This work is concerned with the initiation of SCC in polycarbonate, PC, exposed to an acetone solution. Section 2 describes the polycarbonate and acetone properties and the next Section 3 describes the experimental setup. In Section 4, results are presented and discussed. Two different signs of attack are found on the surface; these are pits and cracks. The distribution of pits and crack patterns are analysed. The way the cracks coalesce, tip to side, is investigated and the finding is supported by stress analysis. A simulation of the growth of multiple cracks is also presented in this section. Last, a few remarks on the present study, followed by the conclusions, are found.

2. Material and preparation

The material used in this investigation is an industrial grade of MACROCLEAR polycarbonate, PC, (Arla plast AB, Sweden), which is a transparent, amorphous and isotropic thermoelastic polymer with Young's modulus $E = 2.3$ GPa, Poisson ratio $\nu = 0.38$, tensile yield stress $\sigma_y = 63$ GPa. The material is used in the as received state, no measures is undertaken to the surface but rinsing with ethanol that is known to react very slowly with PC. During manufacturing, the material is extruded to a plate, and thus a certain degree of anisotropy can not be ruled out, but is not likely. In this study, all specimens are cut in the same direction and no investigation is made for different directions in the material. Residual stresses present in a material due to e.g. manufacturing and preparation can be significant and influence the result. A polariscope is used to determine if any residual stresses are present from the manufacturing and cutting processes. Only specimens without any sign of residual stresses are chosen.

Polycarbonate is chosen due to its comparably high fracture toughness of $K = 3.7$ MPa $m^{1/2}$, Sardinha et al. (2007), compared to other polymers. It is easily machined and prepared. Polycarbonate is also know to be resistant to many chemicals and can in many cases be suitable as substitution to glass in chemical containers. However, a few agents are known to attack and dissolve it. Among the most aggressive is acetone which diffuses easily in PC and dissolves it in a hydrolysis process. Acetone is used in the polymerisation of polycarbonate. The exposure to acetone forces the polymerisation processes to be reversed leading to a defined dissolution of the material. The acetone is supplied by VWR International, Stockholm, Sweden, and is an industrial grade with a purity of at least 99.5%.

The load used in this study is insignificant compared with the toughness of PC and the specimens are only stretched in the elastic region. Without the addition of acetone, no damage can be seen. Polycarbonate is also chosen because it has proven usable in similar studies. Gunnars et al. (1994, 1997) used this material combination to study non-branching crack propagation directions.

3. Experimental setup and procedure

A rectangular test specimen with a length of 100 mm and a width of 20 mm is cut out from a PC plate with the thickness 3 mm using a hacksaw. To avoid crack initiation at the edges, they are polished to a reasonable smoothness and then covered with a protective layer of epoxy glue.

The test specimen is subjected to three point bending. An illustration of a specimen mounted in the test rig is shown in Fig. 1.

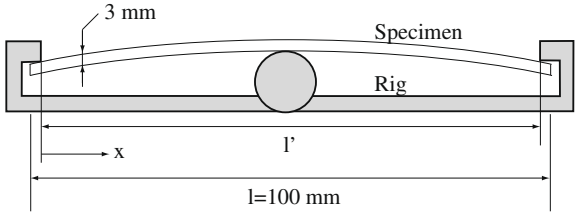

Fig. 1. A side view of a specimen mounted in the three point bend rig. The width of the specimen is 20 mm.

Fig. 2. Overview of a sample surface showing the cracks, and how they are quantified.

With this fixation, the effective test length of the specimen, l', is not the same as the geometrical length, $l = 100$ mm. If nothing else is stated, from now on the meaning of the specimen's length is always referring to the effective length. The whole configuration is submerged into an acetone and water solution. This setup allows study of both sides of the specimen with the exception for the small distance covered by the middle support. The rig is considered as stiff as compared to the specimens, it is made of stainless steel and is not affected by the test solution.

The concentration of acetone and the exposure time is correlated so that the specimens would not break immediately. In the hydrolysis, the acetone solution dissolves the PC, and carbon dioxide and water is produced. Some investigations of this phenomenon have been made by Ghorbel et al. (1995a) and for water by Akele and Thominette (1996). It has been shown that static stresses in the PC drastically accelerates the hydrolysis, cf. Liu et al. (2005) and Ghorbel et al. (1995b). Using the acetone in the received purity of 99.5%, the reaction was too fast to be easily controlled. To this end, the acetone is diluted with distilled water in various proportions to slow the process down and thereby gain better control of the process. A solution with less than 90 wt% acetone renders no visible reaction for times suitable for repeated experiments. In this study, the test pieces are exposed for a time of a few seconds. Solutions with 92 wt% acetone is found to be the most appropriate for this case. This concentration is used merely on empirical basis.

Images of the specimen's surface are collected and examined with an optical microscope. Both sides of a specimen is studied for cracks and pits. The surface is divided into equally sized regions representing all magnitudes of the linearly varying stress on the surface, see Fig. 2. The number of pits is counted in square shaped areas in every region, marked with the number 1, and the number of cracks crossing a straight line, marked with the number 2, is counted in every region. Finally, the total length of the cracks present in every interval is measured. An area density of pits and linear density of cracks can then be calculated at regular intervals along the surface to get a measure of the attack at different stress levels in both compression and tension. The regions are so narrow that the stress can considered to be constant within them.

The micrographs are also used in an attempt to investigate the possibility for the pits to act as crack initiation sites. To this end, the distribution of the cracks is examined and a numerical simulation of the crack growth is performed. It is also noted that the cracks coalesce to form stripes over the sample surface, and the nature of the meetings are looked upon by a FE analysis of the geometry at hand.

4. Results and discussion

4.1. Stress distribution

The type of loading used makes it easy to calculate the stresses on the surface of the specimens. For long slender beams and ideally sharp supports, three point bending gives a linearly varying plane stress state along the surface. The maximum is positioned at the middle of the specimen and zero stress at the outer supports. A FE analysis of the problem at hand confirms that this is true also for a beam of the present dimensions except the parts resting on the middle support. Due to symmetry, only half the beam is shown, the centre part of the beam corresponds to the right hand side of the figures. The FE analysis has been performed using ABAQUS Abaqus, 2003. The result is shown in Fig. 3. The variable x is defined in Fig. 1. In all figures and text, σ, refers to the stress component at the surface parallel to the load. The maximum value is denoted σ_0 and is chosen to be the highest value found at the middle of the beam. The small dip found in Fig. 3 is an artifact due to the finite width and rigidity of the boundary conditions chosen. In reality, the middle support is not so firmly attached. This small effect is neglected and the maximum used is found a small distance away from the geometrical center of the beam, as can be seen in Fig. 3. The normalised stress σ/σ_0 is used in the following.

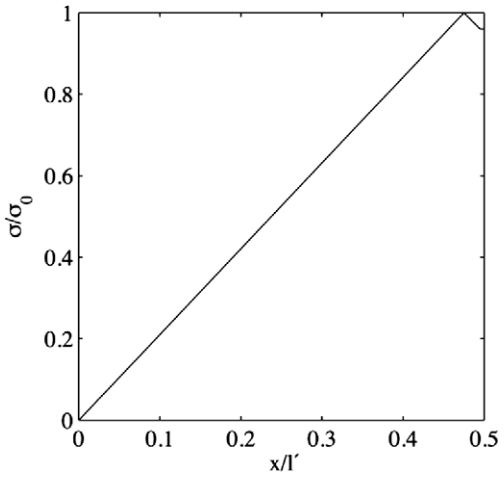

Fig. 3. The stress along the surface in three point bending from FE analysis.

4.2. Pit occurrence

Fig. 4(a) shows a representative part of the surface prior to exposure. On the exposed specimens surface, there is evidence of attack on two different length scales. Fig. 4(b) shows a micrograph of the surface, revealing a roughness in the micrometer domain. At higher magnification, it becomes apparent that the roughness is in fact pits that can be seen as dots on the micrograph. Due to limitations in the optical microscope and the size distribution of the pits, it is hard to determine their size. A typical order of magnitude is a few micrometers but only the number is taken into account, not their size. These pits are assumed to be plausible crack initiation sites. As described in Section 3, the area density, D, of the dots is counted and used as a measure of the severeness of the attack. The normalised dot density, D/D_0 versus σ/σ_0, is shown in Fig. 5. D_0 is the maximum dot density found on the samples. From the figure, it is possible to speculate of a positive stress threshold value of

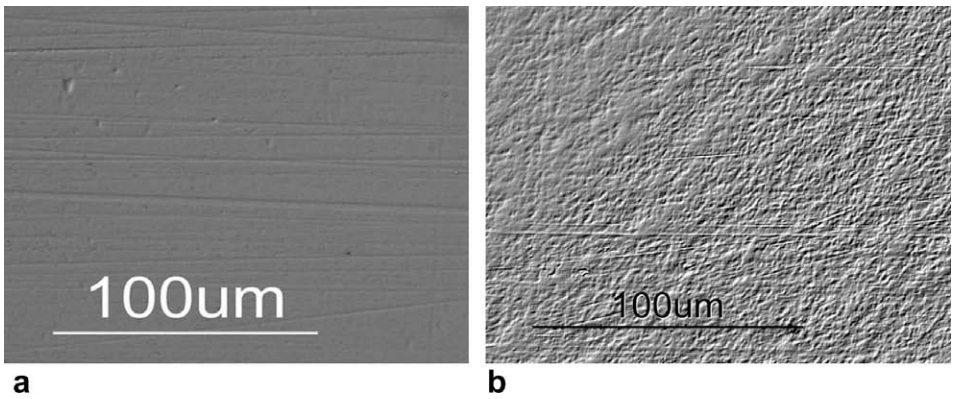

Fig. 4. Typical micrographs of the polycarbonate surface. (a) Before and, (b) after test. The roughness consists of pits seen as dots.

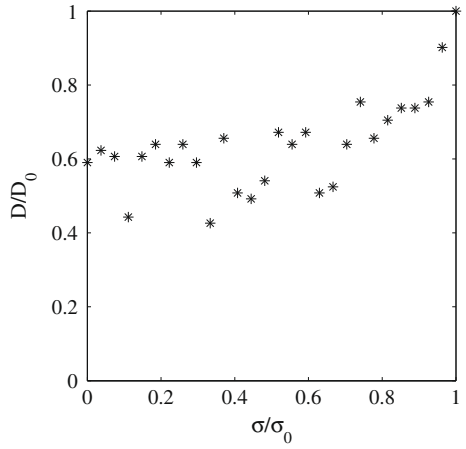

Fig. 5. The area density of dots along the stressed surface.

approximately $\sigma_{th}/\sigma_0 \approx 0.5$, under which only general attack takes place irrespective of load and is also true for negative stress. Above this stress, the PC-acetone interaction seems to have a stress dependent part also.

The pattern of pits can be depicted as a pattern of dots. To find any correlation between the pits, Fourier analysis is employed to search for any characteristic distribution. No preferred distance between the pits can be found. The pits appear to be completely randomly distributed and, at least in areas small enough that the the stress may be considered as constant, no correlation with the ATG instabilities can be found. This may be interpreted as a simultaneous initiation of the pits so they do not have any chance to influence each other and is also an indication that the distribution of pits, in this case, is not an ATG instability phenomena.

4.3. Crack occurrence

On a larger scale, visible to the bare eye, cracks form perpendicular to the load. Fig. 6(a) shows one of these surface cracks. Due to polarization of the light and the stress optical properties of polycarbonate, light or shadow like artifacts in the vicinity of the cracks is visible. At this low magnification, no dots are clearly seen. The number of cracks formed at the surface is counted as a linear density, denoted with N, parallel to the orientation of the load, as described in Section 3. If nothing else is stated, the meaning of a crack is always referring to cracks appearing on the specimen's surface and can be seen as furrows on the specimen transverse to the direction of loading. The length of these furrows is measured, but the penetration depth is not considered. On the surface, many cracks form and grow towards each other. This is seen in Fig. 6(b). Fig. 6(c) shows the corresponding map of crack initiation sites. This will be discussed in the next paragraph. Fig. 7 presents an average of the normalised linear density, N/N_0 along all the specimens' surfaces. N_0 is the maximum crack density. Here, a positive stress threshold value at $\sigma_{th}/\sigma_0 \approx 0.3$ is found for the

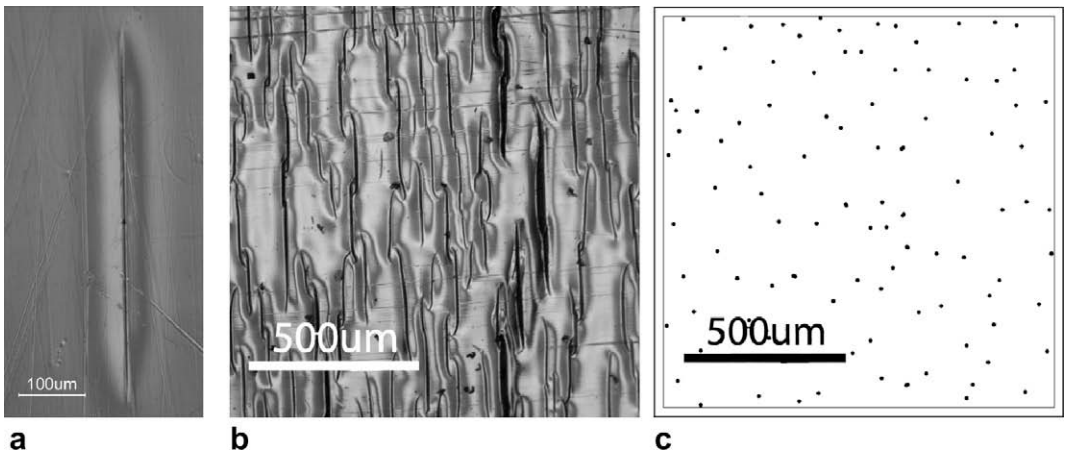

Fig. 6. (a) One crack on a specimens surface. (b) An area used to analyze the distribution of initiation sites. The corresponding map of the initiation sites are indicated in (b) and explicitly shown in (c).

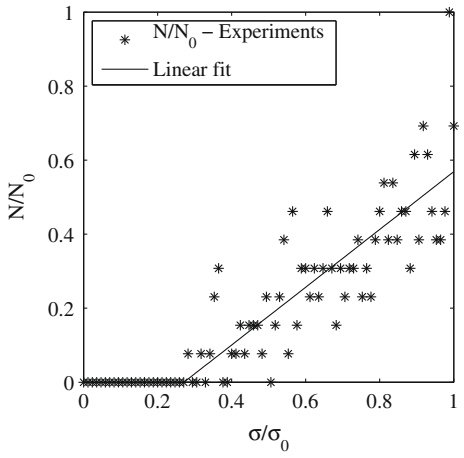

Fig. 7. The linear density of cracks along the stressed surface.

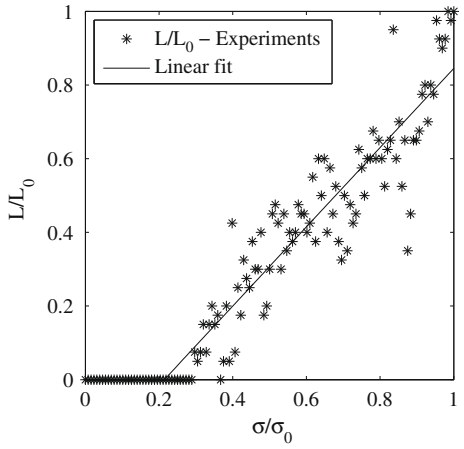

Fig. 8. The total length of cracks along the stressed surface.

formation of cracks. For stress exceeding this value, the density is seen to increase approximately linearly with the stress and no cracks are found for lower and negative stress. The total crack length, L, in each region is measured, cf. Section 3. Fig. 8 shows the relationship of the normalised length L/L_0 and the normalised stress. L_0 is the maximum total length found at the middle of the specimen. It is seen that the length of surface cracks increase linearly with the stress after the stress threshold value is exceeded. Using all data points for N/N_0 and L/L_0 larger than zero, a linear fit of the relationships can be computed for the crack density $N(\sigma) \approx 0.78N_0(\sigma/\sigma_0 - 0.27)$ and crack length $L(\sigma) \approx 1.1L_0(\sigma/\sigma_0 - 0.21)$, respectively. The threshold values for crack formation can be identified in the relationships as 0.21 and 0.27, respectively. It is expected to find these two values to be the same since no crack length can be measured without crack formation. A common threshold value could be found to be approximately 0.25.

It is now of interest to find the origin of the cracks. Here it is assumed that the pits described in Section 4.2 act as initiation sites. Only a fraction of all available pits will grow into cracks and the distribution of these pits is investigated. To find a reasonable location for a initiation point of a crack the following assumptions are made: The cracks are taken to extend with the same rate at both ends, which is a plausible situation not contradicted by any of the experimental results. The crack growth rate is assumed to be constant and independent of stress. Since this is a stress corrosion phenomenon, the rate is controlled by chemical reactions at the crack tips,

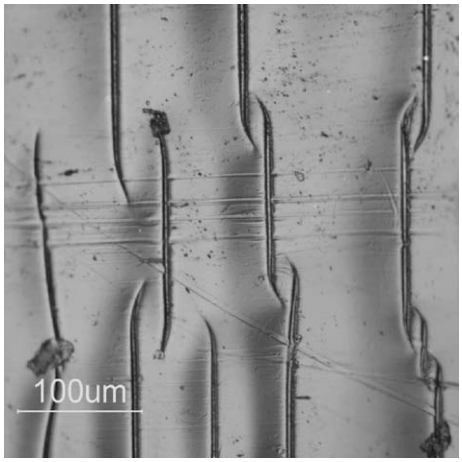

Fig. 9. Close up of the crack tips showing how they are believed to initiate at the center and grow to approach each other and coalesce.

and these are not influenced by the load but rather by the diffusion rate of spices to and from the crack tip region Jones (1992). These assumption will be addressed and used later in Section 4.5. Ostensible conclusions from the given postulates are the choice of taking the centre point of a crack as its origin and define the middle point of a crack as its initiation site. An example of this can be seen in Fig. 6(c) where a map of crack mid points, corresponding to the crack pattern in Fig. 6(b) is depicted. It is seen that a similar random pattern of initiation sites is found as for the pit distribution in general described in Section 4.2. However, a significant difference can be noted in the randomness. A Fourier analysis of the crack initiation site distribution reveals that the pattern is random in nature but the initiation sites are also uniformly distributed and is never seen to be very close together. This is not surprising, since a region around a growing crack exhibits stress relaxation and this indicates some dependence between pits that grow into cracks.

4.4. Crack coalescence

If the cracks are allowed to grow, they will eventually encounter each other. When this happens, they are seen to coalesce to form stripes of cracks across the specimen's surface. The specimen will finally break along these stripes if the exposure is not aborted. In this investigation, the test is always terminated long before that happens. This Section presents experimental results and a finite element stress investigation of the direction of crack growth of two meeting cracks. A special feature can be observed at the point of coalescence. From Fig. 9, it is seen that the crack tips avoid each other. They attract each other first at a point where crack tips from two parallel and meeting crack are approximately at the same position in the direction of crack growth, but they need not necessarily be exactly approaching each other as long as the tips meet close enough to influence each other. The distance between two meeting cracks, for this to happen, is dependent on the crack lengths. The resulting coalescence is formed crack tip to crack side, not tip to tip. This observation is in line with results for co-linear cracks by Melin (1983), who showed that meeting crack tips avoid each other. However, Melin did not consider coalescence. From Fig. 9 it is also apparent that the cracks never coalesce completely, at least not at the surface. A FE analysis of two meeting cracks in a large plate is performed. Fig. 10 shows an illustration of the geometry, but where the distance, d, between the two crack planes is exaggerated compared to the height, h. The crack length $a = h/2$, and $d = a/100$. An external load is applied perpendicular to the crack planes. The symmetry of the stress field in the crack tip re-

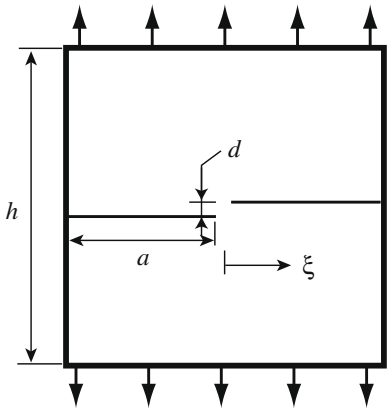

Fig. 10. Geometry and loading used in the FE analysis, $h \gg d$.

gion is investigated. Most cracks, irrespective of process, grow in mode I. In pure mode I load, the stress field is symmetric straight ahead of the crack. A mode II component will tilt the effective stress field and crack path is assumed to change in the same direction. This assumption is adopted also in this case so that the cracks are assumed to grow in the direction of the symmetry of the stress field ahead of the crack tip, see e.g. Broberg (1999). Fig. 11 shows contour plots of the effective stress (von Mises) for three different crack configurations. The three steps are chosen to represent the meeting of two cracks. A change in the stress field is caused by the interaction between the two propagating cracks only, the remote load is kept constant. The crack tips are rounded, since

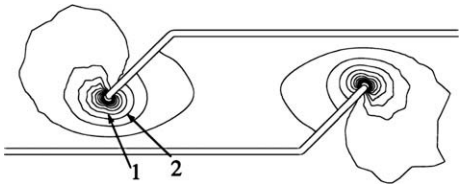

Fig. 13. Contour plot (von Mises) from the FE analysis of two meeting cracks after they have started to attracted each other. The stress levels indicated with 1 and 2 correspond to the same stress level in Fig. 11.

the assumed crack growth mechanism is dissolution, which was discussed earlier. In the first case, where the cracks are approaching each other, $\xi = -d/2$, the stress distribution may indicate that the cracks during continuous growth will turn outwards, avoiding each other. When the crack tips are located at the same horizontal position, $\xi = 0$, the stress field seems quite symmetric around the tips. In the next situation, where the crack tips have passed each other, $\xi = d/2$, the stress distribution is clearly tilted inwards, and thus the cracks are assumed to continue to growth towards each other. This reflects the observed crack pattern, except that no initial outward deviation is observed. However, the assumption of mode I crack growth may not be completely described with the effective stress field. To further explore the position where the cracks start to attract each other is to find the position where the shearing of the crack tip is changing sign. This shearing is due to the mode II component. A displacement ratio between nodes at the crack flanks for the three crack advances shown in Fig. 11, are calculated from the FE analysis according to the difference in

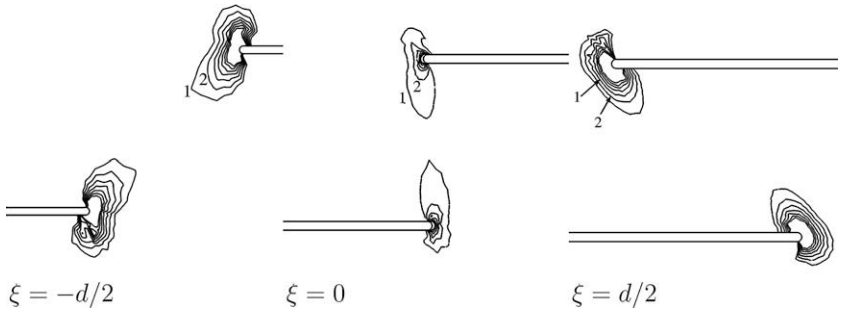

Fig. 11. Contour plot (von Mises) from the FE analysis of two meeting cracks. The variable ξ is defined in Fig. 10. The contours correspond to the same stress level, the numbering indicates where to find the same level of stress, between all sub figures.

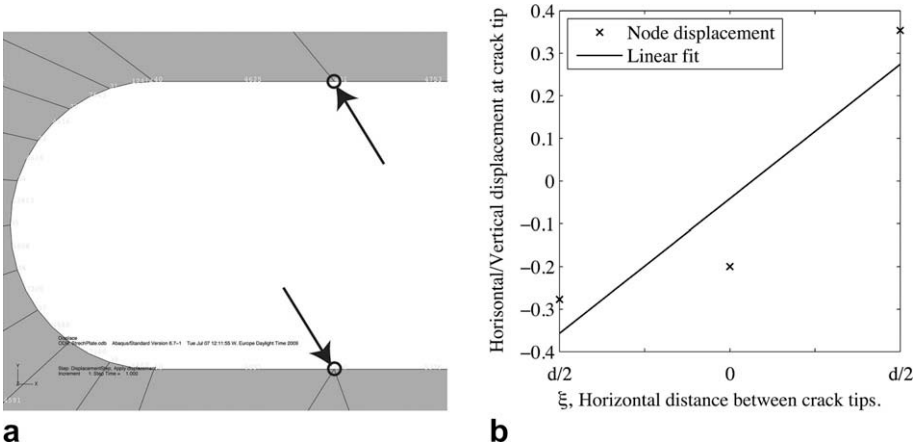

Fig. 12. (a) Nodes used to calculate the displacement ratio. (b) Displacement ratio (×) of nodes marked in (a) at different stages of crack advance, and a linear fit (-).

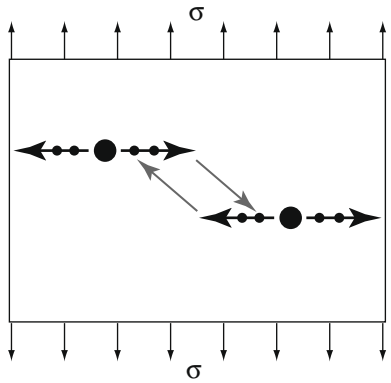

Fig. 14. Schematic view over the crack growth scheme used to simulate the surface crack growth.

displacement in the x-direction divided with the difference in the y-direction. The horizontal distance between the cracks are $\xi = d/2$, 0 and $d/2$, respectively, cf. Fig. 10. The displacement ratios are obtained for the nodes at the crack flanks that are closest to the rounded crack tip, cf. Fig. 12(a). The result is shown in Fig. 12(b), and the shear displacement is found to change sign at approximately $\xi = 0$, as expected. Fig. 13 shows a situation for crack growth when the cracks have started to attract each other and they are approaching one another at an angle, chosen to be 45°. It can be seen from the stress distribution that the cracks may continue to gradually turn towards each other.

4.5. Multiple crack initiation and crack growth simulation

A simulation of the growth of multiple surface cracks is performed, based on the observations and assumptions discussed in previous sections. These are schematically shown in Fig. 14. The surface studied is considered small enough to represent an area where the nominal stress is constant. The side length of the surface under consideration is denoted l_0. The crack growth rate, v_0, is assumed to be constant during a simulation. The crack extends in both directions. The total time of a simulation is denoted t_0, and is divided into constant time increments, Δt. Here, D_t is chosen

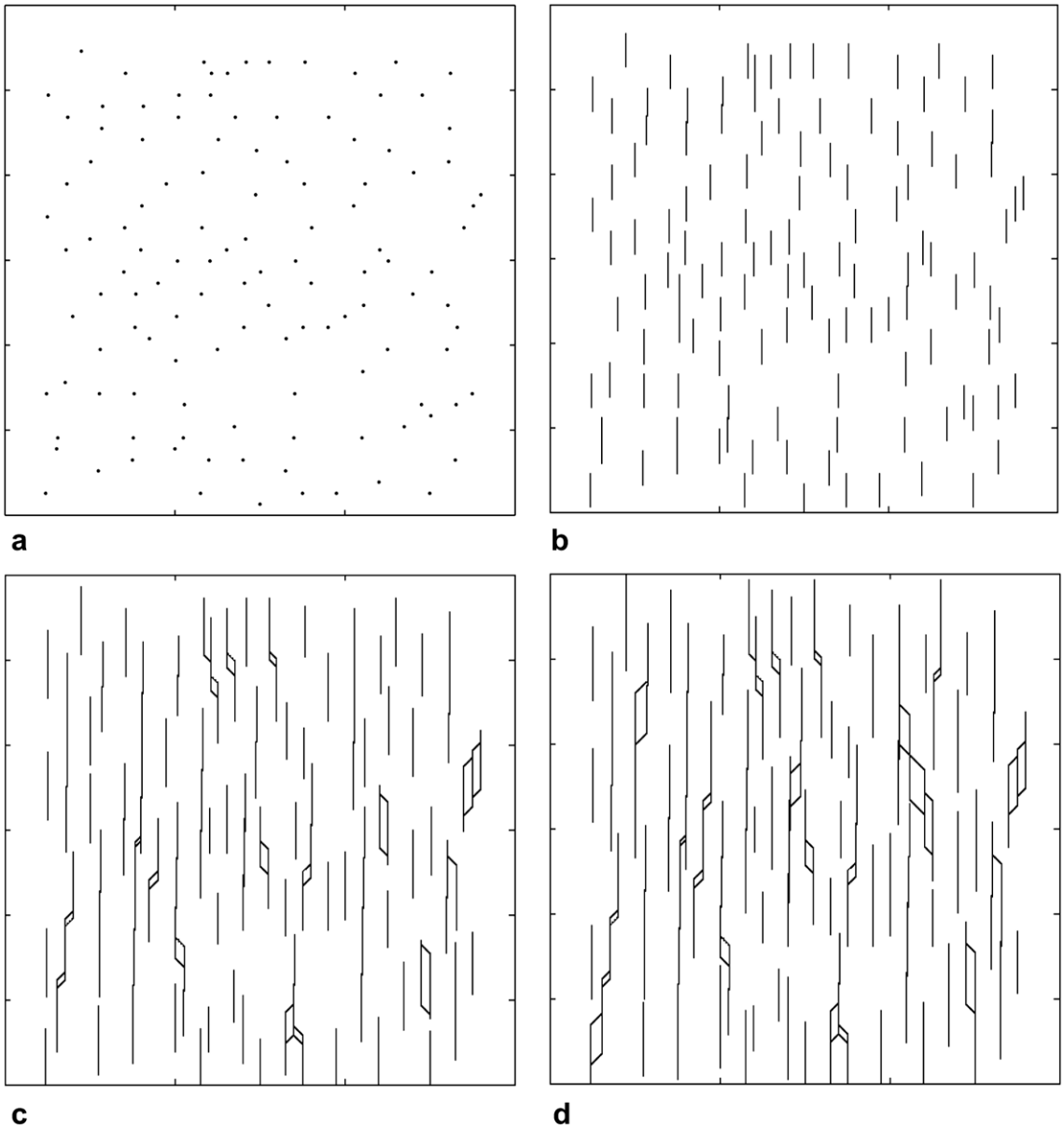

Fig. 15. (a) Initiation sites at the beginning of simulation. (b)–(d) Advancing simulated crack pattern.

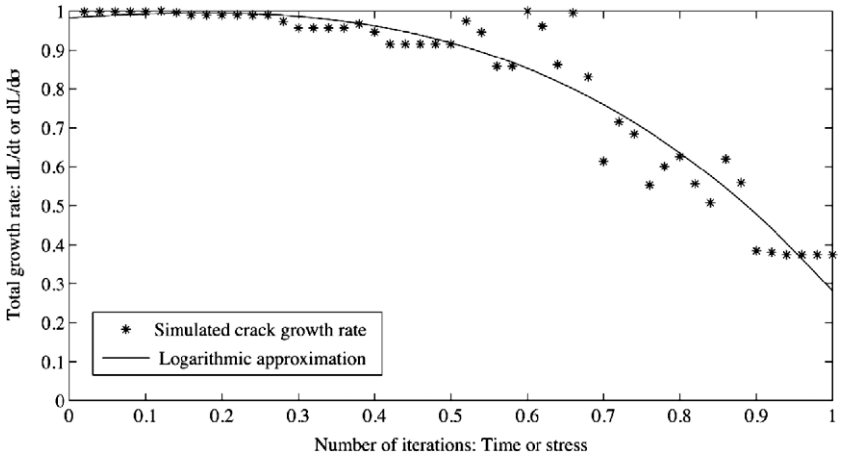

Fig. 16. The crack growth rate is constant until coalescence takes place.

to equal $t_0/500$. This corresponds to that the crack extension at a tip Δl equals $l_0/500$ during one time step. A set of crack initiation points, randomly distributed over a surface, see Fig. 15(a) is taken from an actual set of initiation points found in an experiment. No new initiation sites are created during the simulation.

Before coalescence starts, a crack grows perpendicular to applied load, cf. Fig. 15(b). As soon as two meeting crack tips are perpendicular to or have passed each other, and the distance between them is less than a certain fraction of the sum of crack lengths, each crack turns 45° towards the other. This direction is found plausible from the experimental findings. Thereafter, the path of the cracks is straight again, as illustrated in Fig. 15(c). No stress analysis is performed during this type of simulation and the angle of coalescence is achieved simply by letting the crack tips grow one increment forward and one increment towards the other crack after the requirement for coalescence is fulfilled. The growth direction is governed solely by geometrical considerations. The choice of a deviation angle of 45° seems reasonable with regard to the experimental observations and the results from FE analysis, cf. Figs. 9, 11, 12 and 13. As two cracks coalesce, they are combining into a single crack, whose outer tips are now the only growing crack tips. From Fig. 9, it can be seen that two meeting cracks do not grow together completely. In the analysis, this effect is neglected since the method is not based an analysis of the stresses, as mentioned above, and thus does not change the outcome of the simulation.

The simulated surface crack pattern evolution is shown in Fig. 15(b)–(d). When comparing the crack pattern found in Fig. 6(b) and the simulated pattern in Fig. 15(d), the same characteristics can be found. For example, in Fig. 6(b) it is seen that the distance between a crack tip and the location at its flank, where the other crack meet, increases with the distance for which the two cracks started to interact. However, the tendency to line up and create stripes of cracks is not so pronounced, but can be imagined in some areas. Two meeting crack ends must have reached the same lateral position to be alongside before coalescence can take place, therefore the tips will always miss each other and creat a rhomboidal piece between the cracks when they finally approach each other. This feature is a simple approximation that corresponds to the hook like shape that is seen experimentally.

A consequence of the assumption that the crack growth rate is constant is a decreasing total extension rate, dL/dt, where L is the sum of crack lengths. As more and more cracks coalesce, the number of free ends decreases. According to the assumption of simultaneous initiation, no new cracks initiate to compensate for this decrease. Fig. 16 shows that the total crack growth rate first is constant, and then decreases as more and more coalescence takes place. Crack coalescence, in this case, begins at approximately $t = 0.1t_0$. The decrease is assumed to be logarithmic, and such a curve fitted to the data points is also included in the figure.

Hitherto, the studied area is considered to represent the same spot on a sample, and the evolution of crack pattern is followed with time. However, it may be possible to regard the result of the simulation to reflect a single moment in time for areas experiencing different nominal stress. The density of initiation spots increases approximately linear with stress, as observed from the experiments. Consider the pattern in Fig. 15(d) to represent a part of the sample where stresses are large, and Fig. 15(b) smaller stresses. Since the patterns reflect the situation at one moment, the cracks that have not coalesced must be equally long for both areas. This means that the different figures represent different length scales, equivalent to different time steps. In accordance to the experimental findings, crack coalescence is more probable at larger stress levels simply due to more initiation sites. Thus, Fig. 16 also may represent the total crack length change, L, with nominal stress. However, comparing with the results from the experiments, see Fig. 8, a decrease in L/σ_0, is not observed.

5. Further remarks

On the PC surface, two signs of attack are discovered. A surface roughness, seen as dots, that appears without a threshold stress and also in compression but is seen to have a slight dependence on positive stress. This may mean that the dissolution and degradation process has a stress independent part. On a larger scale, multiple cracks appear on the surface, perpendicular to the stress, but in this case the stress must exceed a positive threshold value so the cracks only appear when the material is stretched and is seen to increase linearly with stress. Since diffusion and dissolution is stress dependent, but also takes place without mechanical load, see Liu et al. (2005), it is plausible to believe that the processes creating these damages are diffusion controlled in some way. The experiments performed by Shreter et al. (2001) in silicon in an etchant shows damage only on one side, as is found in this study also. In that case, attack is not due to dissolution but on dislocation glide and cracks are found on the compressed surfaces instead, as compared with the present study, on the stretched surface. Shreter also found two different signs of attack similar to the ones found here. That is a surface roughness in the nanometre domain and cracks on a larger length scale.

This investigation is made using a light microscope with the possibility to resolve features in the micrometer scale. Shreter used an atomic force microscope, AFM, to detect a roughness in the

nanometre scale. It may be possible to further elaborate this study, taking advantage of an AFM, to find even more detailed information from the surface of the PC and possibly here find a wave pattern correlating to the stress state. In this study, no ATG instability has been found.

When studying and quantifying the surface cracks, only the surface is observed. The cracks are growing, not only on the surface, but also down into the depth of the specimen until it reaches a critical depth where the final failure will occur if the test is not aborted. In these experiments, the crack growth is always aborted long before final fracture occurs. At this stage, all surface cracks are still quite shallow and are not yet significantly affected by any effects due to the depth. This makes it plausible to, as an initial step, analyse only the surface in two dimensions.

The assumptions used in the model for crack growth are subject for corrections to make the simulation more close to the results found in the experiments. The objective here is only to test a few simple rules and these are also to be looked closer upon in a future study.

6. Conclusions

In the present study, characteristics of multiple and chemically assisted initiation and growth of multiple cracks in stressed polycarbonate are studied experimentally. A smooth polycarbonate stripe is exposed to acetone while loaded in three point bending.

- Two signs of attack, in two different length scales, are discovered. Pits form on the surface leading to a roughness. Multiple cracks form perpendicular to the load.
- The pits are seen in the micro meter domain. The cracks are in the millimeter domain, seen by the naked eye.
- The pits are randomly distributed on the surface, indicating a simultaneous formation independent of each other.
- No stress threshold value is found for the formation of pits and only a slight stress dependence is seen.
- The occurrence of cracks is found to have a positive stress threshold value and after that to be stress dependent following a growth law approximately linearly with stress.
- Some of the pits are believed to act as crack initiation sites. These pits are found to have a uniform random distribution.
- In the coalescence of cracks, hooks are seen to form when crack tips meet the other crack's side and not the tip.
- An FE analysis of the stress field of two meeting cracks shows that the cracks may grow to form hooks as is seen in the experiments.
- A numerical simulation of multiple surface crack growth is performed. The resulting crack patterns are similar to those obtained in the experimental. However, the found decrease of the computed average crack growth rate after crack coalescence has started is not supported by the experimental findings.

Acknowledgements

The authors thank Prof. Per Ståhle for valuable discussions and input to the fracture mechanical analysis and Dr. Zoltan Blum at Malmö University for assistance with the polymer chemistry. The financial support from the Knowledge Foundation for the Biofilms – Research Centre for Biointerfaces and the Swedish Research Council (VR 50562401-02, VR 50562402-02) is acknowledged.

References

Davis, J.R. (Ed.), 2001. ASM Handbook, vol. 13. ASM International, Materials Park, Ohio. ISBN 0-87170-007-7.
Jones, H.R. (Ed.), 1992. Stress–corrosion Cracking. ASM International, Materials Park, Ohio. ISBN 0-87170-441-2.
Asaro, J.R., Tiller, W.A., 1972. Interface morphology development during stress corrosion cracking: part I via surface diffusion. Metall. Trans. 3, 1789–1796.
Grinfeld, M.A., 1991. Thermodynamic Methods in the Theory of Heterogeneous Systems. Longman Scientific & Technical, Harlow, New York. ISBN 0-582-06700-6.
Grinfeld, M.A., 1993. The stress driven instability in elastic crystals: mathematical models and physical manifestations. J. Nonlinear Sci. 3, 35–83.
Grinfeld, M.A., 1998. Stress corrosion cracking of an elastic plate. Acta Mater. 46, 631–638.
Spencer, B.J., Voorhees, P.W., Davis, S.H., McFadden, G.B., 1992. The effect of compositionally-generated elastic stresses on morphological instability during directional solidification. Acta Metall. Mater. 40, 1599–1616.
Grinfeld, M.A., 1986. Instability of the separation boundary between a non-hydrostatically stressed elastic body and a melt. Sov. Phys. Dokl. 31, 831–834.
Yang, W.H., Srolovitz, D.J., 1993. Crack like surface instabilities in stressed solids. Phys. Rev. Lett. 71, 1593–1596.
Yu, H.H., 2005. Crack nucleation from a single notch caused by stress-dependent surface reactions. Int. J. Sol. Struct. 42, 3852–3866.
Sou, Z., Yu, H.H., 1997. Crack nucleation on an elastic poly crystal surface in a corrosive environment: low dimensional dynamical models. Acta Mater. 45, 2235–2245.
Spencer, B.J., Meiron, D.I., 1994. Nonlinear evolution of the stress-driven morphological instability in a two-dimensional semi-infinite solid. Acta Metall. 42, 3629–3641.
Kim, K.S., Hurtado, J.A., Tan, H., 1999. Evolution of a surface-roughness spectrum caused by stress in nanometre-scale chemical etching. Phys. Rev. Lett. 83, 3872–3875.
Yu, H.H., Sou, Z. Stress-dependent surface reactions and implications for a stress measurement technique. J. Appl. Phys. 87, 1211–1218.
Grilhé, J., 1993a. Surface instabilities and dislocation formation at the free surface of stressed solids. Europhys. Lett. 23, 141–146.
Grilhé, J., 1993b. Study of roughness formation induced by homogeneous stress at the free surface of solids. Acta Metall. 41, 909–913.
Colin, J., Grilhé, J., 2005. Nonlinear effects of the stress driven rearrangement instability of solid free surfaces. J. Elasticity 77, 177–185.
Song, W., Yang, F., Zhang, J., 2005. Stress-driven evolution of waviness in an elastic layer. Mater. Sci. Eng. A 409, 195–205.
Yang, F., 2006. Stress-induced surface instability of an elastic layer. Mech. Mater. 38, 111–118.
Prevost, J.H., Baker, T.J., Liang, J., Sou, Z., 2001. A finite element method for stress-assisted surface reaction and delayed fracture. Int. J. Sol. Struct. 38, 5185–5203.
Jivkov, A.P., Ståhle, P., 2002. Strain-driven corrosion crack growth – a pilot study of intergranular stress corrosion cracking. Eng. Fract. Mech. 69, 2095–2111.
Jivkov, A.P., 2004. Strain-induced passivity breakdown in corrosion crack initiation. Theor. Appl. Fract. Mech. 42, 43–52.
Ståhle, P., Bjerkén, C., Jivkov, A.P., 2007. On dissolution driven crack growth. Int. J. Sol. Struct. 44, 1880–1890.
Shreter, Y.G., Tarkin, D.V., Khorev, S.A., Rebane, Y.T., 1999. Instability of an elastically compressed silicon surface under etching. Phys. Solid State 42, 1295–1297.
Shreter, Y.G., Rebane, Y.T., Tarkin, D.V., Barakhtin, B.K., Rybin, V.V., 2001. Kinetic mechanism of surface instability evolution during etching, corrosion, and growth of elastically stressed solids. Phys. Solid State 43, 169–175.
Sardinha, N., Weber, R.P., Suarez, J.C.M., 2007. Toughness behavior of gamma-irrated polycarbonate. Polym. Testing 26, 315–355.
Gunnars, J., Delfin, P., Ståhle, P. 1994. Quasi-static curved crack paths in a bi-material specimen obtained by chemical assisted fracture in polycarbonate. Rep. Div. Sol. Mech.
Gunnars, J., Ståhle, P., Wang, T.C., 1997. On crack path stability in a layered material. Comp. Mech. 19, 545–552.
Ghorbel, I., Thominette, F., Spiteri, P., Verdu, J., 1995a. Hydrolytic aging of polycarbonate. I. Physical aspects. J. Appl. Polym. Sci. 55, 163–171.
Akele, N., Thominette, F., 1996. Physical ageing and water sorption in polycarbonate. J. Mater. Sci. Lett. 15, 1001–1002.
Liu, C.K., Hu, C.T., Lee, S., 2005. Effect of compression and thickness on acetone transport in polycarbonate. Polym. Eng. Sci., 687–693.
Ghorbel, I., Thominette, F., Spiteri, P., Verdu, J., 1995b. Hydrolytic aging of polycarbonate. II. Hydrolysis kinetics, effect of static stresses. J. Appl. Polym. Sci. 55, 173–179.
Abaqus, 2003. Abaqus User's Manual Version 6.4. Abaqus Inc., New York.
Melin, S., 1983. Why do cracks avoid each other? Int. J. Fract. 23, 34–45.
Broberg, B., 1999. Cracks and Fracture. Academic Press, London. ISBN 0-12-134130-5.